A Visco-Hyperelastic Constitutive Model to Characterize Both Tensile and Compressive Behavior of Rubber

V. P. W. Shim, L. M. Yang, C. T. Lim, P. H. Law

Impact Mechanics Laboratory, Department of Mechanical Engineering, National University of Singapore, 10 Kent Ridge Crescent, Singapore 119260, Republic of Singapore

Received 11 April 2003; accepted 8 October 2003

ABSTRACT: The strain rate–dependent finite deformation behavior of three types of rubber under tension and compression are experimentally characterized using a Hopkinson bar. Based on the measured data, a frame-independent incompressible visco-hyperelastic constitutive equation is proposed to describe the tensile and compressive responses of rubber under high strain rates. The equation comprises two parts: a three-parameter component based on an elastic strain energy potential, to characterize static hyperelastic behavior, and another with four parameters, developed from the BKZ model, to define rate sensitivity and strain history dependence. Established static and dynamic experimental techniques are employed to determine the seven parameters in the constitutive relationship. Comparison of predictions based on the proposed model with experiments shows that it is able to describe the visco-hyperelastic behavior of rubber-like materials under high strain rates.
 J Appl Polym Sci 92: 523–531, 2004

Key words: dynamic; compression; tension; viscoelastic properties; modeling; rubber

INTRODUCTION

Rubber is commonly employed for vibration isolation, in mechanical energy dissipation devices, and as shock absorbers. It is well known that the mechanical behavior of rubber-like materials is rate dependent.[1,2] Ward[3] and Drozdov and Kolmanovskii[4] have introduced a number of methods to describe rate-dependent behavior. However, experimental data on rubber-like materials have essentially been related to creep, relaxation, or deformation at very low strain rates ($<10°/s$). High deformation rate responses appear relatively less extensively studied. Mechanical properties at high strain rates are difficult to establish and most conventional testing machines use hydraulic actuators only capable of generating low, and at best, intermediate rates of strains (up to the order of 1 s^{-1}). For high strain rate loading, the Split-Hopkinson Bar (SHB) is commonly used and is capable of obtaining stress–strain data with good reliability up to a strain rate of about 10^4 s^{-1}. Rubber is generally compliant; therefore the stress transmitted to the output bar is too small to be detected by normal SHB devices that utilize metallic bars. In the present study, this limitation is overcome by using polycarbonate bars instead of metal ones,[5] so that the difference in mechanical impedance between the bars and rubber is smaller. The stresses transmitted to the output bar are thus sufficiently large to be measured.

Correspondence to: V. P. W. Shim (mpespwv@nus.edu.sg).

Journal of Applied Polymer Science, Vol. 92, 523–531 (2004)

Difficulties encountered in dynamic tensile testing of rubber relate to slippage of specimens from clamps, because of the large strains that can be induced (more than 400%). This may be the reason why there appears to be very little reported on the tensile behavior of rubber under high strain rates. The current investigation involves the design of a specimen-clamping device for tensile SHB tests on soft, compliant materials. The dynamic compressive behavior of rubber-like materials has been studied,[6] where a rate-dependent constitutive equation has been proposed, based on measured stress–strain data; this was subsequently used to simulate the response of rubber under three-dimensional impact loading. However, current test data show that this model, based on compressive test data, is inadequate in describing tensile response. There is therefore a need to develop a description that incorporates both dynamic tensile and compressive behavior. Experiments show that specimens essentially regain their original geometry after unloading and residual strains are negligible, even when the maximum compressive engineering strain induced is larger than 50% and maximum tensile engineering strains exceed 450%. This indicates that the behavior observed is amenable to description by a visco-hyperelastic material model. This study focuses on the formulation of a frame-independent visco-hyperelastic constitutive model to define the behavior of rubber.

EXPERIMENTS

The rubber used in this study is industrially known as Silicone Rubber and comes in various degrees of stiff-

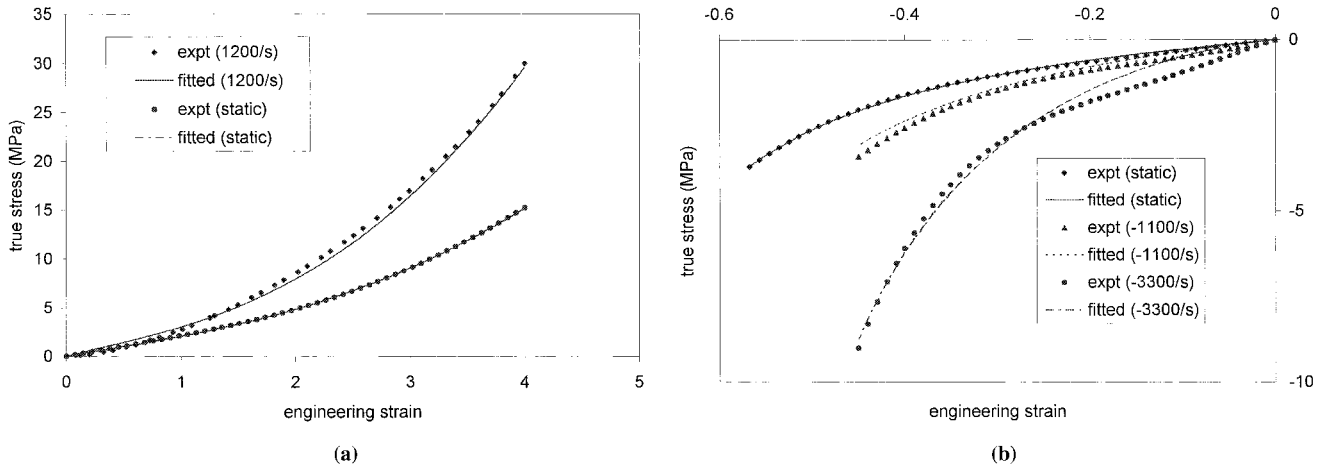

Figure 1 Comparison between theoretical curves and experimental data for (a) SHA40 rubber under tension and (b) SHA40 rubber under compression.

ness, as defined by a Shore Hardness value–e.g., 40, 60, 80–a larger number depicting a higher stiffness. Rubber of three stiffnesses, SHA-40, SHA-60, and SHA-80, were studied; specimens were cut from 2.5-mm-thick sheets measuring 150 mm $\times$ 150 mm. Dies were used to punch out 8-mm-diam. circular discs for compression tests and dog bone–shaped specimens for tensile tests. Quasistatic stress–strain curves for tension and compression were obtained using an Instron universal testing machine. The strain rate induced was about 10^{-2}/s, and the results are shown in Figures 1-3.

For dynamic tensile tests, a modified SHB was used. This comprised a pendulum-based striker and polycarbonate input and output bars. Polycarbonate bars were used to reduce mechanical impedance mismatch with the relatively compliant specimens. A pair of strikers connected to the pendulum made contact with a block connected to the input bar via a short polycarbonate rod, threaded at both ends. This sacrificial piece fractured upon impact, generating an approximately rectangular tensile pulse in the input bar. Polycarbonate adaptors (Fig. 4), designed to hold the specimen, were connected to the input and output bars by screw threads. Specimens were sandwiched between the two halves of component C, which in turn was held in place by component B. Component B was threaded such that, upon tightening into component A, it would squeeze the two halves of component C together, thus gripping the specimen even more tightly. The tensile stress–strain curves obtained from this experimental arrangement are shown in Figures 1(a)—3(a).

Dynamic compression tests were carried out using a Split Hopkinson Pressure Bar (SHPB). Polycarbonate input and output bars were also used, but there was no need for adaptors to clamp the specimens. The dynamic compressive stress–strain curves obtained are shown in Figures 1(b)—3(b).

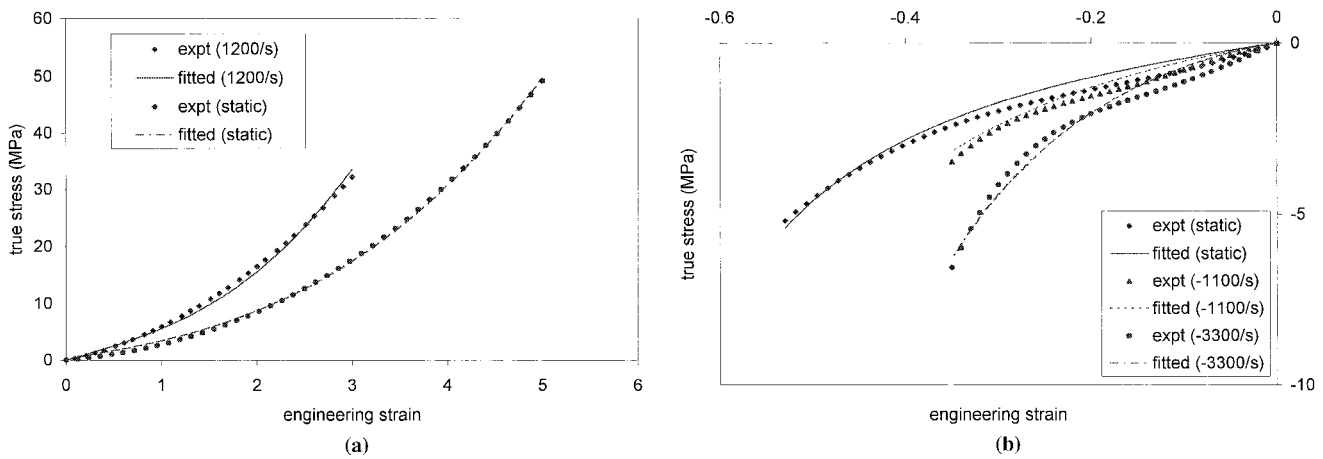

Figure 2 Comparison between theoretical curves and experimental data for (a) SHA60 rubber under tension and (b) SHA60 rubber under compression.

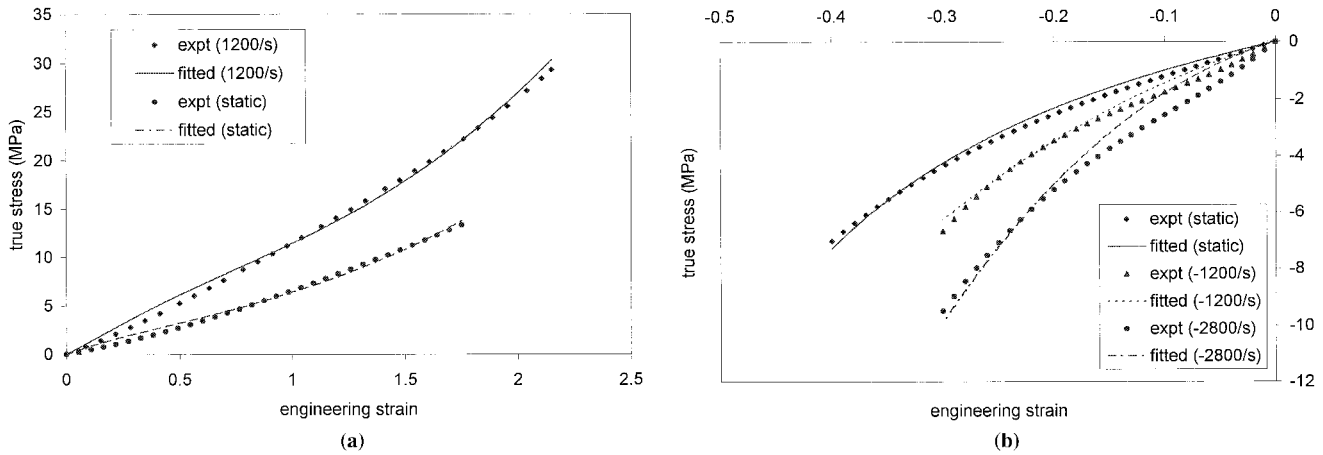

Figure 3 Comparison between theoretical curves and experimental data for (a) SHA80 rubber under tension and (b) SHA80 rubber under compression.

Figures 1–3 show that the behavior of rubber under compression and tension is rate-dependent–there is an enhancement of stress when the deformation rate is increased. Test measurements also show that the residual strain in specimens after unloading is negligible. It is thus expected that a visco-hyperelastic material model is appropriate for characterization of the observed behavior.

HYPERELASTICITY

The rate-independent hyperelastic constitutive equation for rubber under compressive loading, proposed by Yang et al.,[6] is used as a starting point. It is hypothesized that this constitutive model can also be used to characterize tensile behavior.

Consider a point initially located at some position $\mathbf{X}$ in a material. Displacement to a new position $\mathbf{x}$ after deformation results in a deformation gradient $\mathbf{F}$ defined by $\mathbf{F} = \partial\mathbf{x}/\partial\mathbf{X}$. Deformation of the material can be described by the left Cauchy-Green deformation tensor $\mathbf{B}$ $(= \mathbf{F}\cdot\mathbf{F}^{\mathrm{T}})$, or by the right Cauchy-Green deformation tensor $\mathbf{C} = \mathbf{F}^{\mathrm{T}}\cdot\mathbf{F}$), which is related to the Green strain $\mathbf{E} = (\mathbf{C} - \mathbf{I})/2$. The three invariants of $\mathbf{B}$ are defined by: $I_1 = tr(\mathbf{B})$, $I_2 = [I_1^2 - tr(\mathbf{B}^2)]/2$ and $I_3 = \det(\mathbf{B})$. It is reasonable to assume that rubber-like materials are incompressible, which results in $I_3 = 1$.

Following the analysis of Yang et al.,[6] the constitutive relationship for an isotropic incompressible hyperelastic material can be expressed as:[7]

$$\sigma^e = -p_e\mathbf{I} + \alpha_1\mathbf{B} + \alpha_2\mathbf{B}\cdot\mathbf{B} \tag{1}$$

where p_e is the pressure, $\alpha_1 = 2(\partial W/\partial I_1 + I_1\partial W/\partial I_2)$, $\alpha_2 = -2\partial W/\partial I_2$ and σ^e is the Cauchy stress tensor. $W = W(I_1, I_2)$ is a strain energy potential, which is assumed to be representable by a polynomial series involving $(I_1 - 3)$ and $(I_2 - 3)$; it is found that three terms in the polynomial series are sufficient to fit the compressive test data; i.e.

$$W = A_1(I_1 - 3) + A_2(I_2 - 3) + A_3(I_1 - 3)(I_2 - 3) \tag{2}$$

where A_1, A_2, and A_3 are parameters determined via one-dimensional tests. Consider uniaxial loading of a specimen, whereby the stretch in the loading direction is denoted by λ; the principal stretches are $\lambda_1 = \lambda$, $\lambda_2 = \lambda_3 = \lambda^{-1/2}$. The resulting deformation gradient $\mathbf{F}$ and the left Cauchy-Green deformation tensor $\mathbf{B}$ (for uniaxial loading, $\mathbf{B} = \mathbf{C}$) are:

$$\mathbf{F} = \begin{bmatrix} \lambda & 0 & 0 \\ 0 & \lambda^{-1/2} & 0 \\ 0 & 0 & \lambda^{-1/2} \end{bmatrix}, \quad \mathbf{B} = \mathbf{F}\cdot\mathbf{F}^{\mathrm{T}} = \begin{bmatrix} \lambda^2 & 0 & 0 \\ 0 & \lambda^{-1} & 0 \\ 0 & 0 & \lambda^{-1} \end{bmatrix} \tag{3}$$

From eqs. (1) and (2), the expression for stress under uniaxial loading is:

$$\sigma_{11}^e = -p_e + \alpha_1 B_{11} + \alpha_2 B_{11}^2 \tag{4}$$

where $\alpha_1 = 2[A_1 + A_2 I_1 + A_3(I_1^2 - 3I_1 + I_2 - 3)]$, $\alpha_2 = -2[A_2 + A_3(I_1 - 3)]$, and σ_{11}^e is the Cauchy (true) stress. (The engineering stress σ_{11}^0 is related to the true stress by $\sigma_{11}^e = \lambda\sigma_{11}^0$.) The hydrostatic pressure p_e is

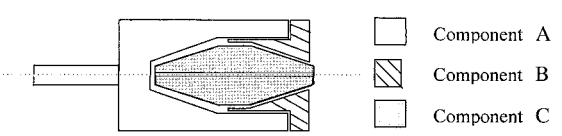

Figure 4 Polycarbonate adapter for dynamic tension tests.

TABLE I
Parameters in Proposed Stress–Strain Equation

Material	A_1 (MPa)	A_2 (MPa)	A_3 (MPa)	A_4 (MPa)	A_5 (MPa)	A_6 (MPa)	A_7 (μs)
SHA40	0.128	0.285	0.0106	0.00125	−0.0451	0.0967	136.6
SHA60	0.174	0.505	0.0299	0.00186	−0.0958	0.176	232.6
SHA80	0	1.451	0.0924	0.00172	−0.470	0.514	285.7

obtained from the condition $\sigma^e_{22} = \sigma^e_{33} = 0$, together with the relation $B_{22} = B_{11}^{-1/2}$:

$$\sigma^e_{22} = 0 = -p_e + \alpha_1 B_{11}^{-1/2} + \alpha_2 B_{11}^{-1} \tag{5}$$

This constitutive relationship, applied to one-dimensional loading, is defined by combining eqs. (4) and (5); this can be written as a function of the stretch λ,

$$\sigma^e_{11} = 2\lambda(1 - \lambda^{-3})\{A_1\lambda + A_2 + A_3[I_1 - 3 + \lambda(I_2 - 3)]\} \tag{6}$$

The relationship between stretch λ and engineering strain ϵ_{11} in the direction of the uniaxially applied load is $\lambda = 1 + \epsilon_{11}$. Stress–strain curves from quasistatic compression and tensile tests, as shown in Figures 1–3, are used to determine the parameters in eq. (6), by adopting a simple least squares approach. Values of the parameters A_1, A_2, and A_3 for the three grades of rubber are presented in Table I. Comparisons between the theoretical curves and test data, expressed in terms of true stress and engineering strain, are shown in Figures 1–3. The good correlation exhibited for all three materials substantiates the validity of the proposed hyperelastic constitutive equations in describing the compressive and tensile responses of rubber-like materials.

VISCO-HYPERELASTICITY

It is postulated that visco-hyperelastic behavior arises from a combination of hyperelasticity and viscoelasticity, whereby the total stress is the sum of these components, i.e.,

$$\sigma = \sigma^e + \sigma^v \tag{7}$$

where σ^e is the quasistatic hyperelastic response defined by eq. (1) and σ^v characterizes the rate-dependent properties of the material.

Characterization of rate-dependent behavior

A primary characteristic of viscoelastic materials is the effect of previous deformation; the stress state depends on the strain and/or strain rate histories. The constitutive relationship for a homogeneous, isotropic, and incompressible material can be expressed in the following form:[8]

$$\sigma^v = -p^v + \mathbf{F}(t) \cdot \overset{t}{\underset{\tau=-\infty}{\mathbf{\Omega}}} \{\mathbf{C}(\tau)\} \cdot \mathbf{F}^T(t) \tag{8}$$

where σ^v is the Cauchy stress tensor, p^v is the pressure in the viscoelastic material, and $\mathbf{\Omega}$ is a matrix functional that describes the effect of strain history on stress; this relationship for σ^v is frame-independent. Approximations to represent the functional $\mathbf{\Omega}$ have been proposed for solids and these are described in the work by Lockett[8] and more recently by others (e.g.,[4,9]). From these studies, a significant result was that relatively few parameters are needed to model finite strain viscoelastic material behavior. A number of nonlinear viscoelastic constitutive models have been introduced in the monograph by Carreau et al.[9] An area of focus with respect to viscoelastic models is to simplify the function $\mathbf{\Omega}$; for example, the BKZ model[10,11] and its applications.[12] The rate-dependent functional $\mathbf{\Omega}$ approximated by the BKZ model has the following form:

$$\mathbf{\Omega}_{\text{BKZ}} = \mathbf{I} \int_{-\infty}^{t} A(t-\tau) \frac{d}{d\tau} tr(\mathbf{E}(\tau))\, d\tau + 2 \int_{-\infty}^{t} B(t-\tau)\dot{\mathbf{E}}(\tau)\, d\tau \tag{9}$$

where A and B are functions of time and strain rate is defined by $\dot{\mathbf{E}} = \frac{1}{2}\dot{\mathbf{C}} = \frac{1}{2}(\dot{\mathbf{F}}^T \cdot \mathbf{F} + \mathbf{F}^T \cdot \dot{\mathbf{F}})$ and $(d(tr(\mathbf{E}(t)))/dt = \frac{1}{2}\dot{I}_1^C$, where I_1^C is the first invariant of $\mathbf{C}$.

It is assumed that the functions $A(t)$ and $B(t)$ have the same form depending on the argument, namely:

$$A(t) = 2A_5 m(t) \quad \text{and} \quad B(t) = A_6 m(t) \tag{10}$$

where A_5 and A_6 are constants and the relaxation function $m(t)$ decreases with t. In general, $m(t)$ is an exponential series described by :

$$m(t-\tau) = \sum_{i=1}^{N} \exp\left(-\frac{t-\tau}{\theta_i}\right) \tag{11}$$

where θ_i is the relaxation time. Note that the response of a Maxwell material model is described by an exponential term and eq. (11) can be considered as the response of several Maxwell elements connected in parallel. N has been assigned a value of 2 by several researchers,[13,14] whereby one relaxation time is used to describe behavior at low strain rates ($10^{-4} \sim 10^{-1}$/s) and another to characterize behavior at high strain rates ($10^2 \sim 10^3$/s); this is designated as the "ZWT" model. In the version proposed by Osaki et al.[15] a value of $N = 5$ was assumed, while Wagner[16] selected $N = 8$. It has been reported[17] that the relaxation times depend on the microstructure of the material. Motion within the microstructure, which determines the relaxation time, is activated by a corresponding loading rate. From the viewpoint of the macromechanical behavior of materials, the relaxation time recorded in a test depends on the loading time or rate. For many polymeric materials deformed at strain rates generated by conventional SHPB devices, the mechanical response can be adequately described by a single relaxation time.[13,14] In general, a good material model would not require an excessive number of parameters to describe the essential features of the material. Hence, in this study, only one relaxation time is used in eq. (11); i.e., $N = 1$.

Time is taken with reference to the instant loading commencement and it is assumed that the effect of deformation history on stress for $\tau < 0$ is ignored. Thus, the deformation history considered to affect the stress response–i.e., the limits of integration in the second term in eq. (9)–become $[0,t]$ rather than $(-\infty, t]$. Substituting eqs. (10) and (11) with $N = 1$ into eq. (9) results in the following proposed integral approximation for $\mathbf{\Omega}_{\mathrm{BKZ}}$,

$$\overset{t}{\underset{\tau=-\infty}{\mathbf{\Omega}}}_{\mathrm{BKZ}}\{\mathbf{C}(\tau)\} = \int_0^t [A_5 \dot{I}_1^C(\tau)\mathbf{I} + 2A_6\dot{\mathbf{E}}(\tau)]\exp\left(-\frac{t-\tau}{A_7}\right) d\tau \tag{12}$$

where A_7 is a relaxation time, a material constant. For incompressible materials, such as rubber in this investigation, the pressure in material may be undefined. Thus, eq. (12) which defines $\mathbf{\Omega}_{\mathrm{BKZ}}$, is modified by replacing the unit tensor $\mathbf{I}$ with $\mathbf{C}/I_1^C$ to approximate the response of incompressible materials:

$$\overset{t}{\underset{\tau=-\infty}{\mathbf{\Omega}}}\{\mathbf{C}(\tau)\} = \int_0^t \left[A_5 \frac{\dot{I}_1^C(\tau)}{I_1^C}\mathbf{C} + 2A_6\dot{\mathbf{E}}(\tau)\right]\exp\left(-\frac{t-\tau}{A_7}\right) d\tau \tag{13}$$

The relationship between the matrix functional $\mathbf{\Omega}$ and strain rate for one-dimensional stress and constant strain rate conditions is now examined. The engineering strain rate, which is the same as the stretch rate $\dot{\lambda}$, is related to the strain rate by $\dot{\mathbf{E}}_{11} = \lambda\dot{\lambda}$, and to the rate of the first invariant of $\mathbf{C}$ by $\dot{I}_1^C = 2\lambda(1 - \lambda^{-3})\dot{\lambda}$. Thus, for one-dimensional loading, eq. (13) yields:

$$\Omega_{11} = 2A_7\lambda\dot{\lambda}\left[A_5\frac{(\lambda^3-1)}{(\lambda^3+2)} + A_6\right]\left[1 - \exp\left(-\frac{t}{A_7}\right)\right] = f(\lambda)\dot{\lambda}\left[1 - \exp\left(-\frac{\lambda-1}{\dot{\lambda}A_7}\right)\right] \tag{14}$$

where $f(\lambda) = 2\lambda A_7\{A_5[(\lambda^3 - 1)/(\lambda^3 + 2)] + A_6\}$ and $t = (\lambda - 1)/\dot{\lambda}$ for a constant stretch rate. Equation (14) shows that curves describing how Ω_{11} varies with $\dot{\lambda}$ for a constant λ should be convex; i.e., $(\partial\Omega_{11}/\partial\dot{\lambda})|_{\lambda=\mathrm{const}} > 0$ and $(\partial^2\Omega_{11}/\partial\dot{\lambda}^2)|_{\lambda=\mathrm{const}} < 0$. Eqs. (8), (9), and (14) show that Ω_{11} is the stress component that describes strain rate sensitivity, and the characteristics of the $\Omega_{11} \sim \dot{\lambda}$ relationship should therefore be similar to that of $\sigma_{11} \sim \dot{\lambda}$. Consequently, the convex property of Ω_{11} described by eq. (14) should be observed in the stress—strain rate curves derived from experiments. However, this feature is not supported by the present test results. From the experimental stress–strain curves in Figures 1–3, curves of stress as a function of stretch rate can be obtained and are displayed in Figures 5(a–c) for the three types of rubber. These show that, in contrast to what is expected from eq. (14), curves of stress versus stretch rate are concave; i.e., $(\partial\sigma_{11}/\partial\dot{\lambda})|_{\lambda=const} > 0$ and $(\partial^2\sigma_{11}/\partial\dot{\lambda}^2)|_{\lambda=const} \geq 0$. Thus, it is questionable whether eq. (14) [deduced from eq. (13)] is suitable for describing the rate-dependent behavior of the rubber tested. Consequently, eq. (13) should be modified so that a higher order of stretch rate dependence is used to characterize the observed behavior. Furthermore, Figures 1–3 show that the compressive behavior is much more rate-sensitive than the tensile response for a common magnitude of engineering strain (e.g., for engineering strains less than 50%, the dynamic and static tensile stresses are quite similar, whereas dynamic compressive stresses are notably higher than quasistatic values). In the light of present test data, this model [defined by eq. (13)] is inadequate in describing the rate dependence of the various grades of rubber examined. Therefore, a new variant must be introduced to characterize the difference in the rate-dependent response between tension and compression; this is done via the functional $\mathbf{\Omega}$. It is noted that the time derivative of the second invariant of $\mathbf{C}$, $\dot{I}_2^C = 2(1 - \lambda^{-3})\dot{\lambda}$, can describe rate-dependent behavior that is more sensitive to compression than tension for any given magnitude of engineering strain. Consequently, the following relationship, based on the preceding analyses, is proposed to characterize the behavior of rubber in the present study:

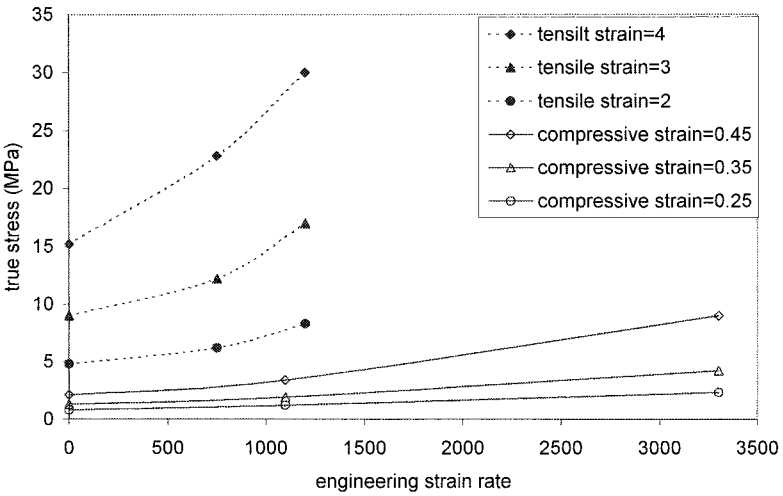

(a)

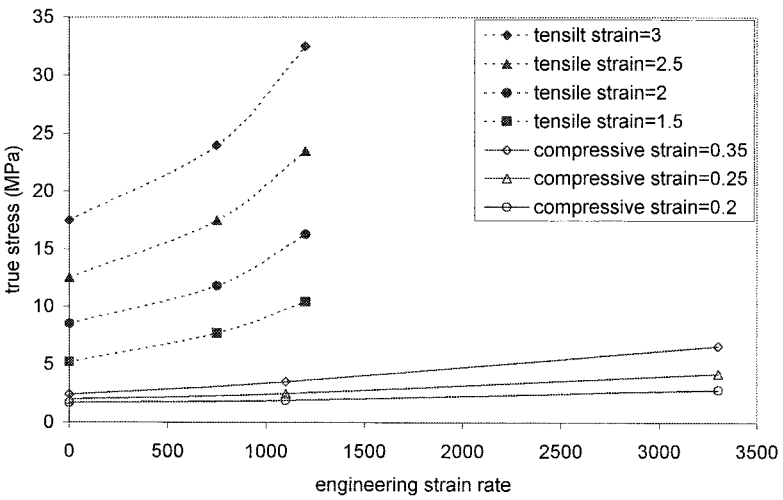

(b)

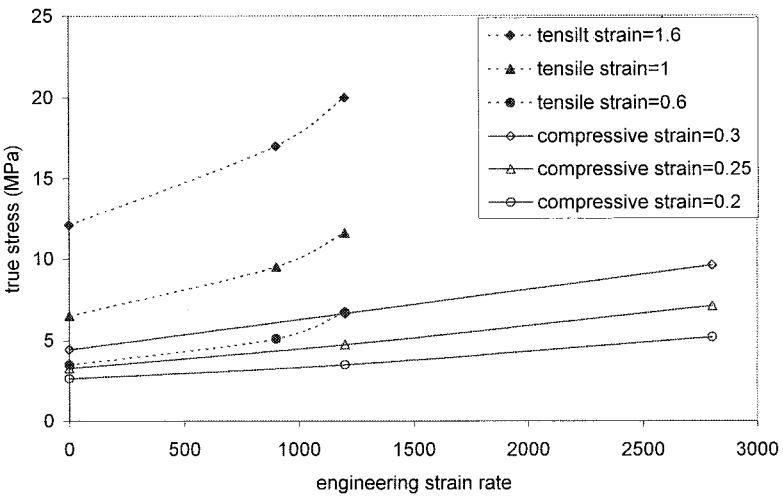

(c)

Figure 5 Variation of true stress with engineering strain rate for a common engineering strain: (a) SHA40; (b) SHA60; (c) SHA80.

$$\overset{t}{\underset{\tau=-\infty}{\Omega}}\{\mathbf{C}(\tau)\} = (1 + A_4\dot{I}_2^C)\int_0^t \left[A_5\frac{\dot{I}_1^C(\tau)}{I_1^C}\mathbf{C} + 2A_6\dot{\mathbf{E}}(\tau)\right]\exp\left(-\frac{t-\tau}{A_7}\right)d\tau \quad (15)$$

where A_4 is another material parameter.

Substitution of eq. (15) into eq. (8) yields a frame-independent finite strain viscoelastic constitutive relationship for incompressible materials.

$$\boldsymbol{\sigma}^v = -p^v\mathbf{I} + (1 + A_4\dot{I}_2^C)\mathbf{F}(t)\cdot\left[\int_0^t\left[A_5\frac{\dot{I}_1^C(\tau)}{I_1^C}\mathbf{C} + 2A_6\dot{\mathbf{E}}(\tau)\right]\exp\left(-\frac{t-\tau}{A_7}\right)d\tau\right]\cdot[\mathbf{F}(t)]^T \quad (16)$$

Visco-hyperelasticity

A combination of eqs. (1), (16), and (1) yields:

$$\boldsymbol{\sigma} = -p\mathbf{I} + \alpha_1\mathbf{B} + \alpha_2\mathbf{B}\cdot\mathbf{B} + (1 + A_4\dot{I}_2^C)\mathbf{F}\cdot\left(\int_0^t\left[A_5\frac{\dot{I}_1^C(\tau)}{I_1^C}\mathbf{C} + 2A_6\dot{\mathbf{E}}(\tau)\right]\exp\left(-\frac{t-\tau}{A_7}\right)d\tau\right)\cdot\mathbf{F}^T \quad (17)$$

where p ($= p^e + p^v$) is the total pressure comprising static and viscoelastic components. A_i, ($i = 4\ldots7$) are material parameters that characterize the viscoelastic response under high strain rates and are determined from tests involving dynamic uniaxial loading of specimens. For uniaxial loading, $\dot{E}_{11} = \lambda\dot{\lambda}$, $\dot{I}_1^C = 2\lambda(1 - \lambda^{-3})\dot{\lambda}$ and $\dot{I}_2^C = 2(1 - \lambda^{-3})\dot{\lambda}$. Substitution of these relations into eq. (17) yields the stress-deformation relationship for the direction of loading:

$$\sigma_{11} = -p^v + \sigma_{11}^e + (1 + 2A_4(1 - \lambda^{-3})\dot{\lambda})\lambda^2\int_0^t 2\lambda\left[A_5\frac{\lambda^3-1}{\lambda^3+2} + A_6\right]\exp\left(-\frac{t-\tau}{A_7}\right)\dot{\lambda}\,d\tau \quad (18)$$

where σ_{11}^e is described by eq. (6) and p^v is determined from the condition that the transverse stress $\sigma_{22} = 0$, allowing it to be written as:

$$p^v = (1 + 2A_4(1 - \lambda^{-3})\dot{\lambda})\lambda^{-1}\left(\int_0^t\lambda\left[2A_5\frac{(1-\lambda^{-3})}{\lambda^3+2} - A_6\lambda^{-3}\right]\exp\left(-\frac{t-\tau}{A_7}\right)\dot{\lambda}\,d\tau\right) \quad (19)$$

Substitution of the preceding expression for p^v into eq. (18) yields the relationship between stress and deformation in the direction of loading.

$$\sigma_{11} = \sigma_{11}^e + (1 + 2A_4(1 - \lambda^{-3})\dot{\lambda})\lambda^2\int_0^t 2\lambda\left[A_5\frac{\lambda^3-1}{\lambda^3+2} + A_6\right]\exp\left(-\frac{t-\tau}{A_7}\right)\dot{\lambda}\,d\tau - (1 + 2A_4(1 - \lambda^{-3})\dot{\lambda})\lambda^{-1}\int_0^t\lambda\left[2A_5\frac{(1-\lambda^{-3})}{\lambda^3+2} - A_6\lambda^{-3}\right]\exp\left(-\frac{t-\tau}{A_7}\right)\dot{\lambda}\,d\tau \quad (20)$$

where the rate of stretching is equal to the engineering strain rate; i.e., $\dot{\lambda} = \dot{\varepsilon}_{11}$. Dynamic uniaxial tests were conducted on SHA40, SHA60, and SHA80 rubber specimens. For SHA40 rubber, data corresponding to average strain rates of 1,200/s, −1,100/s, and –3,300/s (the negative sign denotes compression) were used to determine the parameters A_i ($i = 4\ldots7$) via a least squares fit. The values of these parameters are given in Table I and a comparison between the fitted curves and test data is shown in Figure 1. Substitution of the values of A_i into eq. (20) facilitates the prediction of stress–strain responses at high strain rates. Validity of the proposed model is confirmed by conducting a dynamic tensile test at a strain rate of 750/s and comparing the experimental data with the curve generated by eq. (20). Figure 6 shows very good correlation.

It should be noted that the values of A_5 for the three types of rubber listed in Table I are negative. Under one-dimensional stress conditions, the term affected by A_5, [i.e., $A_5\,[\dot{I}_1^C(\tau)/I_1^C]\mathbf{C}$ in eq. (17)) is $2A_5\lambda(\lambda^3 - 1/\lambda^3 + 2)\dot{\lambda}$, which is negative for both tensile and compressive loading when A_5 is negative; also its magnitude increases with deformation rate $\dot{\lambda}$. Consequently, the influence of this term, arising from deformation rate, is such that the stress magnitude is enhanced for compression but reduced under tension. This confirms that the negative value of A_5 obtained is consistent with experimental observations (Figs. 1–3), particularly that the compressive response is much more rate sensitive than the tensile response for a given magnitude of engineering strain.

To further substantiate applicability of the analysis to rubber of other hardnesses, the same procedure is adopted for SHA60 and SHA80 rubber. One dynamic tensile and two dynamic compressive experimental stress–strain curves from SHB tests were again used to determine the parameters A_i ($i = 4\ldots7$). The average strain rates of the curves used for this were 1,200/s, −1,100/s, and –3,300/s for SHA60 rubber, and

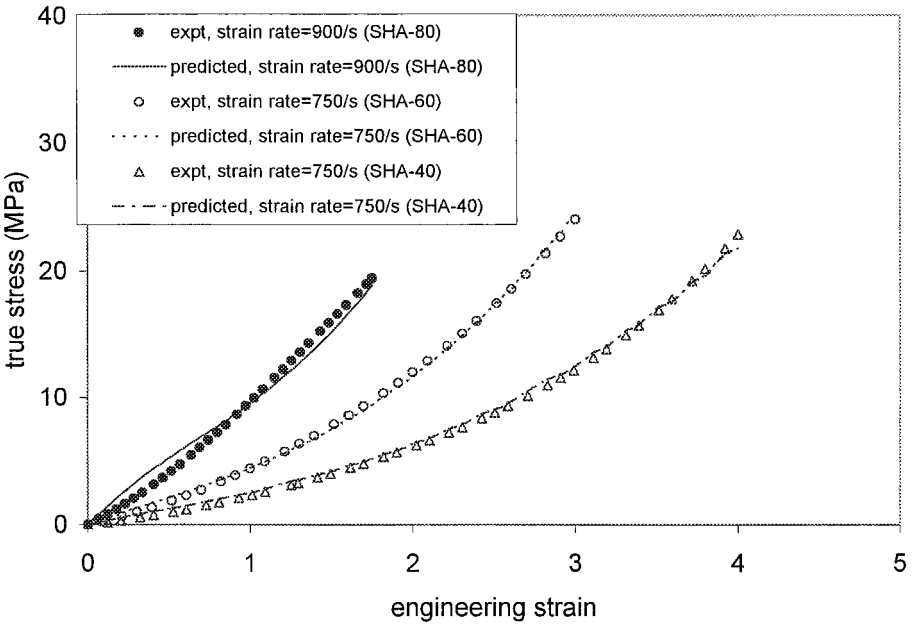

Figure 6 Comparison between predicted and experimental stress—strain responses at high strain rates.

1,200/s, −1,200/s, and –2,800/s for SHA80 rubber. The resulting values of A_i ($i = 4 \ldots 7$) are also shown in Table I. Comparisons of the respective fitted theoretical curves with test data for SHA60 and SHA80 rubber are shown in Figures 2 and 3. Again, confirmation of the validity of the proposed constitutive relationship is provided by comparing predictions with experiments. Substitution of the values of A_i into eq. (20) facilitates prediction of stress–strain responses at a (high) strain rate of 750/s for SHA60 rubber and at 900/s for SHA80 rubber. These comparisons between predicted curves and test data are also shown in Figure 6 and demonstrate that the proposed model is well suited for the description of visco-hyperelastic behavior of rubber-like materials loaded at high strain rates.

CONCLUSION

The tensile and compressive behavior of three types of rubber was experimentally characterized over a range of strain rates: $10^{-2} \sim 10^{3}$ /s. Stress–strain data shows that the mechanical properties of rubber are viscoelastic (strain rate dependent). By employing a fundamental approach to the formulation of constitutive relationships and using the BKZ model as a reference, a novel constitutive equation was proposed to describe the visco-hyperelastic behavior of incompressible rubber-like materials under both tension and compression. Static response is accommodated by an expression comprising a hyperelastic relationship based on an elastic strain energy potential. A three-term truncated series for this potential was found to adequately describe hyperelasticity of the material. Another expression, developed from the BKZ model, was introduced to characterize viscoelastic response under high strain rates, where the relaxation response is described by a Maxwell element and the strain rate dependence is nonlinear. Combining the expressions yielded a hyperelastic solid in parallel with a nonlinear viscoelastic element, thus characterizing not only hyperelasticity but also strain rate–dependent viscoelasticity. Stress–strain curves generated by the model for three kinds of rubber were compared with static and dynamic experimental data. The comparisons show that the proposed model is well suited for the description of visco-hyperelastic behavior of rubber-like materials loaded at high strain rates not only under compression but also under tension.

References

1. Johnson, A. R.; Quigley, C. J. Rubber Chem Technol 1992, 65, 137–153.
2. Johnson, A. R.; Quigley, C. J.; Freese, C. E. Comput Methods Appl Mech Eng 1995, 127, 163–180.
3. Ward, I. M. Mechanical Properties of Solid Polymers; John Wiley & Sons: New York, 1983.
4. Drozdov, A. D.; Kolmanovskii, V. B. Stability in Viscoelasticity; Elsevier: New York, 1994.
5. Rao, S.; Shim, V. P. W.; Quah, S. E. J Appl Polym Sci 1995, 66, 619–631.
6. Yang, L. M.; Shim, V. P. W.; Lim, C. T. Int J Impact Eng 2000, 24, 545–560.

7. Rivlin, R. S. Proceedings of the First Symposium of Naval Structural Mechanics; Pergamon: Oxford, 1960; pp. 169–198.
8. Lockett, F. J. Nonlinear Viscoelastic Solids; Academic Press: New York, 1972.
9. Carreau, P. J.; De Kee, D. C. R.; Chhabra, P. R. Rheology of Polymeric Systems: Principles and Applications; Hanser Publishers: New York, 1997.
10. Bernstein, B.; Kearsley, A.; Zapas, L. J. Trans Soc Rheol 1963, 7, 391–410.
11. Bernstein, B.; Kearsley, A.; Zapas, L. J. Rubber Chem Technol 1965, 38, 76–89.
12. Tanner, R. I. J Rheol 1988, 32, 673–702.
13. Wang, L. L.; Yang, L. M. Progress in Impact Dynamics; Wang, L. L.; Yu, T. X.; Li , Y. C., Eds.; Univ. of Science and Technology of China: Hefei, China, 1992; pp. 88–116.
14. Wang, L. L.; Huang, D.; Gan, S. In Constitutive Relation in High/Very High Strain Rates; Kawata, K.; Shioiri, J., Eds.; IUTAM Symposium: Noda/Japan, 1995; pp. 137–146.
15. Osaki, K.; Ohta, S.; Fukuda, M.; Kulata, M. J Polym Sci 1996, 14, 1701–1715.
16. Wagner, M. H. Rheol Acta 1979, 18, 33–50.
17. Ferry, J. D. Viscoelastic Properties of Polymers; John Wiley & Sons: New York, 1980.